Flood Inundation Extraction and its Impact on Ground Subsidence Using Sentinel-1 Data: A Case Study of the "7.20" Rainstorm Event in Henan Province, China

Qianye Lan, Jie Dong, Shangjing Lai, Nan Wang, Lu Zhang, and Mingsheng Liao

***Abstract*—On July 20, 2021, the northern Henan Province was hit by a historically rare, exceptionally heavy rainstorm ("7.20" Rainstorm Event), accompanied by severe urban flooding, flash floods, landslides, and other multiple disasters, resulting in significant casualties and property losses. On the other hand, the long-term overexploitation of groundwater since the last century has led to severe ground subsidence in the same area. We apply the intensity information of Sentinel-1 SAR images to extract the large-scale flood inundation area and their phase information to measure the ground deformation. Since heavy precipitations can recharge groundwater, the relationship between flood inundation, groundwater level change, and ground deformation is analyzed. The results show that the flood inundation areas are mainly distributed along the major rivers due to river overflowing, while heavy precipitation led to the rise of groundwater levels, and there was a significant amount of subsidence mitigation and surface uplift across the region due to the groundwater recovery. This study demonstrates the contribution of radar remote sensing to analyze the mechanism of groundwater recharge and subsidence mitigation benefited by rainstorm events and provides a technical reference to similar circumstances.**

***Index Terms*—Extreme precipitation events, ground deformation, InSAR, water level change.**

I. Introduction

FLOODS are among the most common and devastating natural disasters, known for their deadly and destructive impact [1]. While various factors can lead to floods, heavy rainfall is the most prevalent cause. In recent years, due to global warming, the climate in northern China has become increasingly warm and humid, with frequent rainstorms in summer. Around July 20, 2021, a particularly severe rainstorm, referred to as the "7.20" Rainstorm Event, affected the north and central parts of Henan Province. According to the China Meteorological Administration, the recent heavy rainfall is primarily attributed to the abundant moisture brought by Typhoon In-fa. Influenced by the terrain, precipitation intensified on the windward slopes. In addition, the low stability between the subtropical high-pressure system in the western Pacific and the continental high-pressure system in central Henan contributed to large rainfall amounts, concentrated rainfall periods (mainly on July 20), and high precipitation intensity. From July 17 to 23, the average precipitation in the province was 223 mm, with 285 stations reporting measurements exceeding 500 mm. The daily rainfall at over 20 national weather stations exceeded the historical extreme [2]. Following China's meteorological standards, precipitation ranging from 50 to 99.9 mm within 24 h is classified as "heavy rain," while precipitation between 100 and 249.9 mm is termed "torrential rain," and amounts exceeding 250 mm are referred to as "extraordinary torrential rain." According to information from the official website of the Henan Provincial Hydrological and Water Resources Survey and Reporting Center, from 8:00 a.m. on July 17 to 8:00 a.m. on July 24, Henan Province experienced widespread heavy to torrential rain, with the cities of Anyang, Hebi, Xinxiang, and Jiaozuo receiving heavy rain and torrential rain, and some areas facing extraordinary torrential rain. The extreme precipitation unleashed widespread flooding across many cities, resulting in a wide range of damage and substantial disaster-related losses [3], [4].

Emergency monitoring of floods is essential for rescue and postdisaster reconstruction. Of great importance is the identification of the spatial distribution of flooding areas. Remote sensing technology has emerged as an indispensable tool for disaster monitoring due to its capacity for large-scale observations. Cloud cover could prevail during flood events. Synthetic aperture radar (SAR) remote sensing offers significant advantages, such as being unaffected by weather conditions and penetrating through clouds. This compensates for the limitations of optical remote sensing, which struggles to observe the ground surface in cloudy weather. Various water surface extraction and flood detection methods have been developed by combining

Manuscript received 16 October 2023; revised 15 November 2023 and 8 December 2023; accepted 22 December 2023. Date of publication 1 January 2024; date of current version 16 January 2024. This work was supported in part by the National Natural Science Foundation of China under Grant 42374013, and in part by the National Key Research and Development Program of China under Grant 2023YFC3009400 and Grant 2021YFB3900604-03. *(Corresponding author: Jie Dong.)*

Qianye Lan, Shangjing Lai, Nan Wang, Lu Zhang, and Mingsheng Liao are with the State Key Laboratory of Information Engineering in Surveying, Mapping and Remote Sensing, Wuhan University, Wuhan 430079, China (e-mail: lanqye@whu.edu.cn; laishangjing@whu.edu.cn; wangnannan@whu.edu.cn; luzhang@whu.edu.cn; liao@whu.edu.cn).

Jie Dong is with the School of Remote Sensing and Information Engineering, Wuhan University, Wuhan 430079, China (e-mail: dongjie@whu.edu.cn).

Digital Object Identifier 10.1109/JSTARS.2023.3348845

polarization, texture, coherence, and radiometric properties of SAR images [5], [6], [7], [8], [9].

Floods, in addition to their destructive nature, can bring abundant water resources, providing a significant recovery of local groundwater in the short term under the appropriate conditions. Most of northern Henan Province is in the North China Plain (NCP), an area of chronic water scarcity with large regions of overexploited groundwater. Long-term overexploitation of groundwater has triggered ground subsidence [10], [11], [12], which tends to weaken the city's ability to carry natural disasters and may have a fatal impact on buildings and infrastructures.

Multitemporal SAR interferometry technology has widely been used to monitor large-scale ground deformation with millimeter-level measurement precision [13], [14], [15], [16], [17]. Different methods were developed, including permanent scatterers InSAR and small baseline subset (SBAS) [18], [19]. The NCP is one of the significant subsidence areas in China, and there have been many previous studies of NCP subsidence using InSAR. Shi et al. found that the distributions of subsidence in the NCP are spatially consistent with that of deep groundwater depression cones [20]. Li et al. and Dong et al. used InSAR to obtain the distribution of surface deformation in the Northern Henan Plain and the whole Henan Province in 2017–2018 and 2018–2020, respectively, and analyzed the cause of subsidence [21], [22].

Ground subsidence occurs slowly and gradually, but once it happens, it is irreversible and difficult to control. Restrictions on groundwater extraction and groundwater recharge are essential and efficient ways to mitigate local ground subsidence [10], [23], [24], [25]. Numerous international experiments have been conducted to study the relationship between changes in the groundwater level and deformation evolution [26], [27], [28], [29], [30]. Rainstorms and floods can recharge the local groundwater, relieving ground subsidence caused by groundwater overexploitation.

SAR images contain intensity and phase information that can be used to extract flood inundation and surface deformation, respectively, and help reveal the relationship between the two. The use of InSAR, which can measure surface deformation over a wide range, is of interest in helping to study the mechanism of the "7.20" Rainstorm Event and flooding impact on ground subsidence. Therefore, we first use Sentinel-1 intensity images to extract the flood inundation area after the event. Then, we employ the phase information to measure the surface deformation in northern Henan from January 2020 to April 2023. Finally, using multisource observation data, we assess the impacts of torrential rainfall and floods on the groundwater level and surface deformation.

II. Study Area and Data Used

A. Study Area

The study area covers the region between 34°48′38″ ∼ 37°01′16″E, 112°33′48″ ∼ 116°05′50″N, including Handan in Hebei Province and Anyang, Hebi, Puyang, Xinxiang, and Jiaozuo in Henan Province. With the Taihang Mountains to the west, the NCP takes up the entire region to the east, and the Yellow River to the south, the terrain is overall high in the west and low in the east.

The study area has a warm temperate continental monsoon climate with four distinct seasons and uneven seasonal distribution of precipitation, with 80% of the yearly rainfall concentrated in the summer months of June, July, and August. The significant increase in rainfall during the summer months is prone to flooding, which is also the flood season of the rivers in this area. The main rivers are shown in Fig. 1. Weihe River upstream mountains steep, fast-flowing, and downstream through the plains, the water flow is gentle, with low excretion capacity. During the flood season, floods are often diverted along the Communist Canal and other slope depressions, and flooding is frequent on both sides of the river. Large-scale water conservancy projects, such as the Yuecheng Reservoir in the Zhanghe River Basin, have been constructed and have played a role in managing floods.

The study area possesses abundant groundwater resources. The area around the Taihang Mountains in Hebi, Xinxiang, and Jiaozuo has a high degree of karst development and contains a large amount of karst water. Furthermore, the foothills of the Taihang Mountains exhibit abundant fractured karst water. This fractured karst water is replenished through direct or indirect infiltration of atmospheric precipitation, and it demonstrates a rapid recharge rate. Alluvial flood loose deposits primarily cover the study area's vast plains. The groundwater in these areas is predominantly composed of porous water in loose rock formations, with a widespread distribution and abundant water quantity. As the aquifer extends from the mountainous region toward the plains, the single-layer thickness gradually decreases, the number of layers increases, and the particle size transitions from coarse to fine [21]. The lack of surface water but the abundance of groundwater in the region and its large population has led to a major dependence on groundwater for industrial and agricultural production. Since the mid-1980s, the scale and intensity of groundwater exploitation have increased significantly, resulting in serious overexploitation of groundwater and the formation of regional ground subsidence funnels.

Various mineral resources are distributed in the front belt of the Taihang Mountains, among which coal mines are the most economically valuable minerals in Henan Province. Hebi and Jiaozuo are famous for their coal resources.

B. Satellite SAR Data

A total of 390 scenes of two paths (paths 40 and 113) C-band ascending Sentinel-1 (S1) data were used, acquired between January 2020 and April 2023. The coverage area is presented in Fig. 1. S1 has four imaging modes; the interferometric wide mode we used has a resolution of 5 × 20 m and a swath width of 250 km. The repeat cycle of S1 is 12 days. Table I lists the S1 data parameters we used for the water surface extraction and deformation monitoring. In addition, ALOS precise digital 3-D map (AW3D) with 30 m resolution from the Japan Aerospace Agency was used as an external DEM data aid for processing.

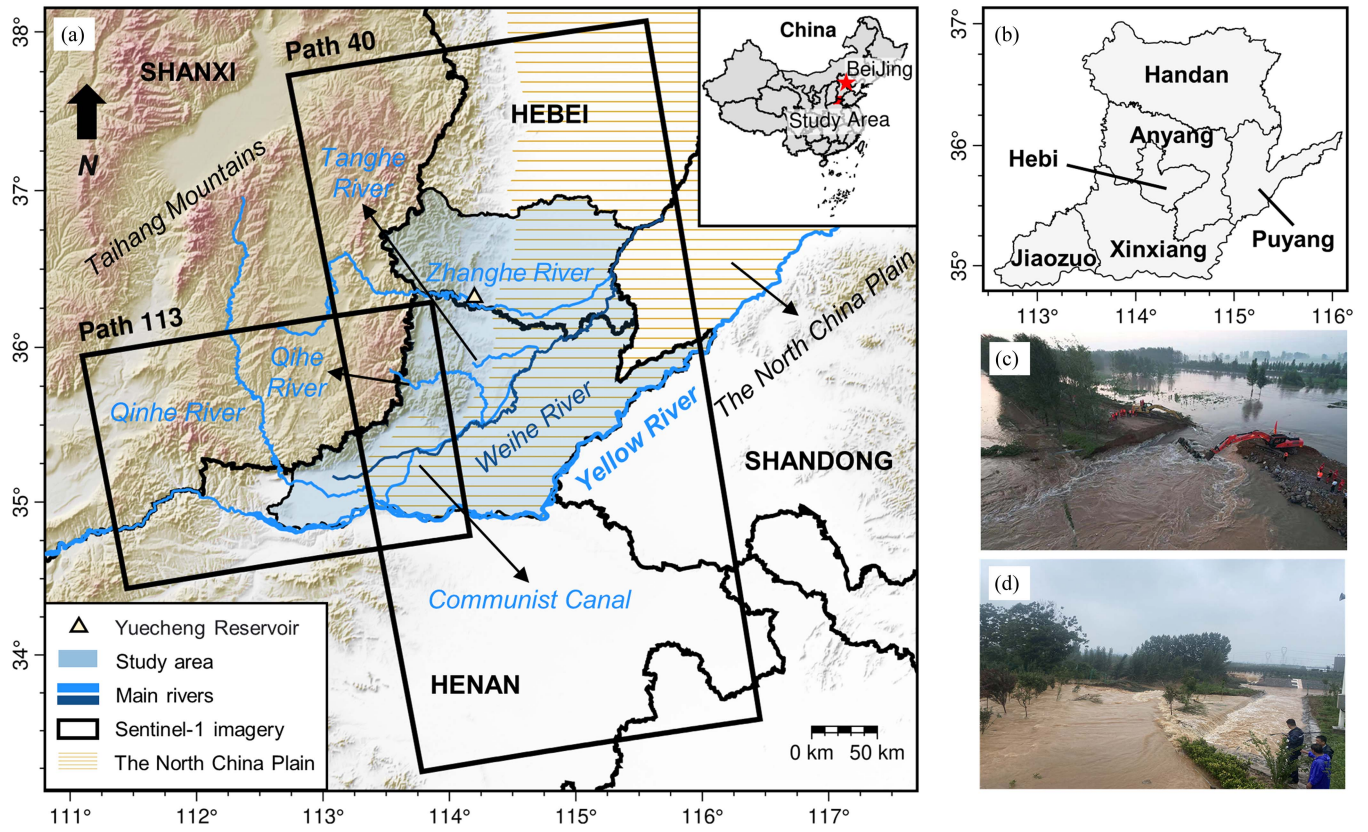

Fig. 1. Study area. (a) Geographical location and its hydrology and topography. (b) Administrative division of the study area. (c) Site of sealing the breach of the Weihe River after it broke at 19:00 on July 22, 2021. (d) Location of flood control of the South-to-North water diversion project located at the junction of Huixian and Weihui in Xinxiang City, on July 22, 2021. Pictures are from www.thepaper.cn.

TABLE I
MAIN PARAMETERS OF THE S1 SAR DATASETS USED

	Path	Temporal coverage	Polarization	Image No.
Water surface extraction	113	July 8, 2021, and August 1, 2021	VH	6
	40	July 15, 2021, and July 27, 2021	VH	6
Deformation detection	113	January 3, 2020 – April 24, 2023	VV	93
	40	January 10, 2020 – April 17, 2023	VV	297

C. Groundwater Level Data

We use two types of groundwater data. The first is the groundwater level monitoring well data for the NCP for January 2020 to December 2021 from the China Geological Survey. We used groundwater level data with one measurement every five days. The second is the monthly water report from the Water Resources Department of Henan Province, which includes each month's change in the average groundwater level in the plains of the province compared to the previous month, as well as the range of changes in the average groundwater level in each city.

III. METHODOLOGY

To assess the impact of flooding on the northern part of Henan Province, we use the intensity and phase of SAR images to obtain the flood inundation areas and surface deformation, respectively, with the flowchart shown in Fig. 2.

A. Flood Inundation Extraction Using SAR Intensity

Flooding area extraction is primarily water surface identification. The thresholding algorithm is a widely used and less time-consuming technique [31], [32], [33], [34]. Considering the advantages of thresholding, we use it to extract flood inundation areas and refine it using a high-resolution DEM product.

Initial extraction of water bodies from a single SAR intensity image can be done quickly using the thresholding method. Water surfaces, especially inland ones with less wind disturbance, have low backscatter intensity in the microwave band and show a deep dark color in intensity images, which is distinctly different from other features. We obtained SAR intensity images less affected by speckle noise by multilooking and Refined Lee filtering [35]. Since the area of nonwater bodies in the region is much larger than that of the water body, it is difficult to form an apparent bimodal feature in the gray histogram of the processed SAR intensity map. We take the region of interest for the water surface of each image separately for grayscale value statistics to get the grayscale range of the water body and take the maximum value

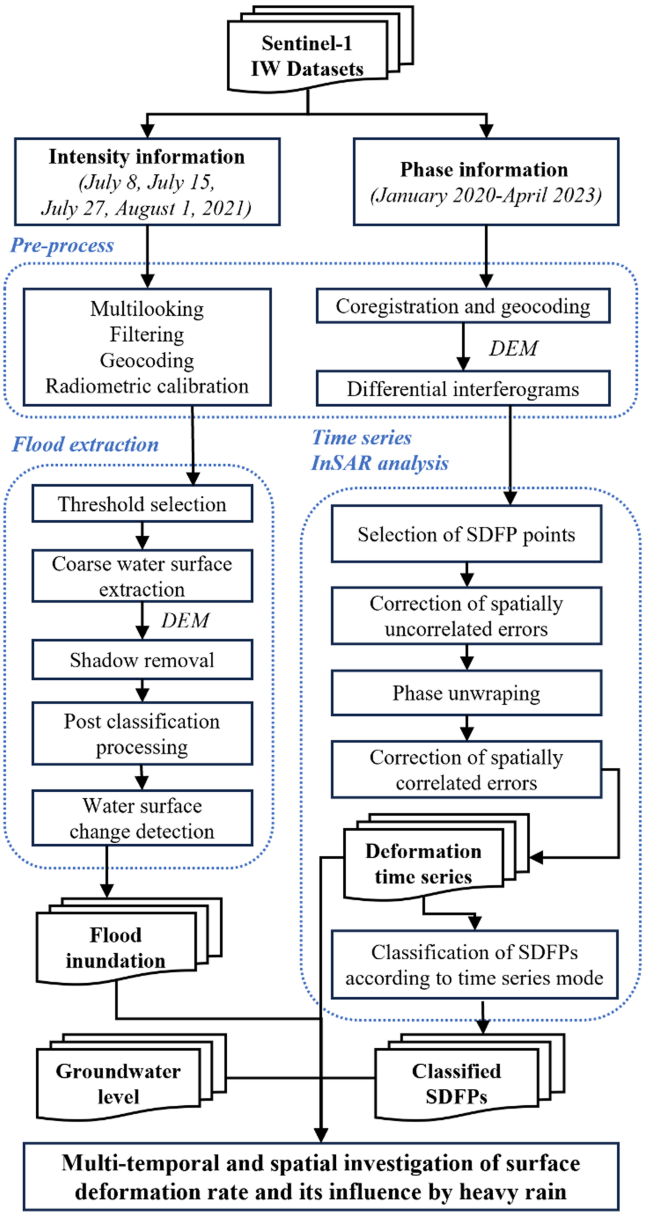

Fig. 2. Flowchart of methodology.

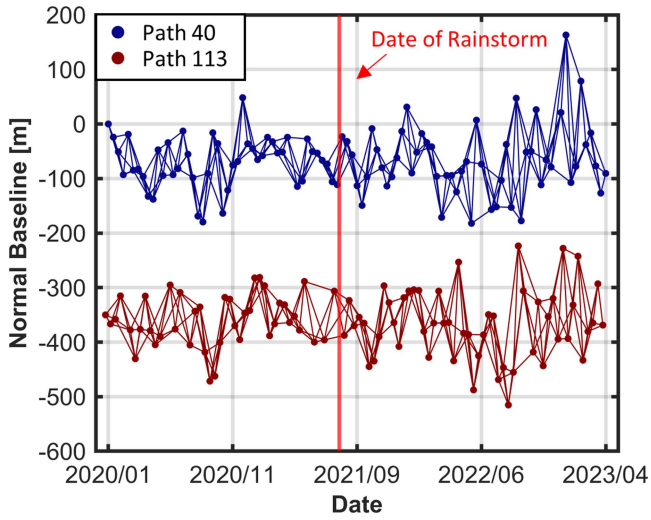

Fig. 3. Temporal and spatial baselines of the two S1 paths. The red vertical line indicates the rainstorm date July 20, 2021. The maximum spatial baseline is 300 m, and the maximum temporal interval is 90 days.

as the segmentation threshold for the coarse extraction of the water surface.

Due to the imaging characteristic of SAR imagery, mountain shadows with low backscattering intensity may be mistakenly extracted. Slope thresholds were set using external DEM information to form a mountain mask to remove the inaccurately extracted mountain shadows from the coarse water extraction result. The majority analysis is applied to the classification to improve the extraction results. We defined the transform window size as 3×3. We replaced the category of the central image element with the category of image elements that are predominant in the transform window to remove specks.

Water surfaces were extracted separately from the images whose dates are the closest to the storm before or after. Comparing the spatial distribution of water bodies on the before and after dates, it is considered that the area of increased water surfaces on the poststorm date is the area of flooding due to the rainstorm.

B. Surface Deformation Measurement Using SAR Phase

We used GAMMA software [36] to preprocess SAR images before time series InSAR analysis. After coregistration and geocoding, interferogram pairs can be obtained using the SBAS baseline connectivity idea. SBAS method maintains a high coherence by selecting suitable spatial and temporal baseline thresholds to form interferometric pairs. Fig. 3 shows the interferometric pairs of the two S1 datasets. A differential interferogram is obtained by removing the flat and topographic phases from the interferogram. The phase ϕ_{int} of a pixel in the differential interferogram can be describe as follows [13], [18]:

$$\phi_{\text{int}} = W\{\varphi_{\text{def}} + \varphi_{\text{atm}} + \varphi_{\text{orb}} + \varphi_{\text{DEM}} + \varphi_{\text{noise}}\} \quad (1)$$

where φ_{def} is the phase change caused by the displacement of the surface target in the line-of-sight (LOS) direction during the two acquisitions, φ_{atm} denotes the phase of atmospheric delay, φ_{orb} stands for phase generated by orbital uncertainty, φ_{DEM} is the error caused by DEM inaccuracy, and φ_{noise} is the noise phase. All phase components except the deformation phase contained in the differential interferogram are removed using the StaMPS method [37]. Slowly decorrelation filter phase (SDFP) points are chosen during the time series InSAR analysis, whose phase decoherence manifests more slowly over a short period [38]. The time series deformation along the LOS is obtained on the SDFPs. Since only ascending S1 data are available, we convert the deformation along the LOS direction into the vertical direction with the assumption that only vertical deformation exists.

After obtaining the flood inundation and surface deformation using S1 datasets, a comprehensive analysis is carried out by combining the flood inundation, the surface deformation, and the groundwater level data to evaluate the impact of the "7.20" Rainstorm Event and flooding on the ground subsidence.

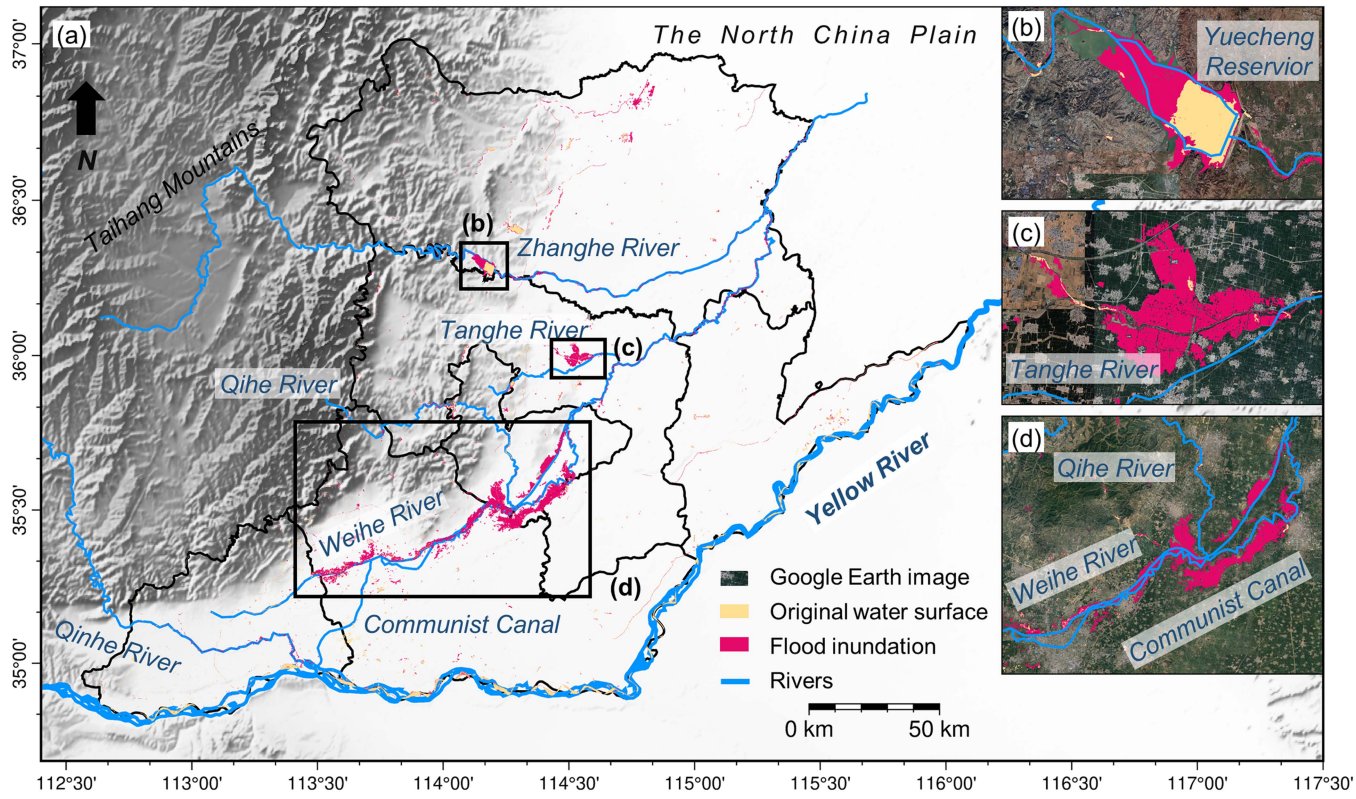

Fig. 4. (a) Flood inundation areas. Prestorm and poststorm S1 images are listed in Table I. (b), (c), and (d) are zoomed-in images of three distinct flooded areas, respectively, whose geographic locations are shown in (a). The optical image backgrounds of (b), (c), and (d) are all from Google Earth.

IV. Results and Analyses

A. Extraction of Flood Inundation Area

The result of flood inundation area extraction is shown in Fig. 4. Small water bodies have been removed to highlight the location of water changes. From July 20 to 22, 2021, Henan Province was affected by the rainstorm and the water surface expanded significantly, flooding approximately 546.2 km^2 in the study area. The flooding area is distributed along the Weihe River, Communist Canal, Qihe River, and Tanghe River basins. Meanwhile, the area of the Yuecheng Reservoir increased significantly. During the rainstorm, reservoirs were dispatched to help control the flooding.

According to relevant information [39], since the first half of July, there have been many rainfalls in Henan Province, the Weihe River, the Communist Canal, the Qihe River, and other major rivers generally rose in water level. The rainstorm of Henan in the July 2021 period was primarily concentrated in Xinxiang and Hebi, the time period was mainly focused on the 21st from 7:00 pm to 9:00 pm. According to the information in the relevant reports, on the evening of July 22, 2021, the Communist Canal not far west of the Weihe River overflowed with floodwaters into the Weihe River. On the morning of July 23, the Hebi section of the Weihe River had burst its banks. Nearby villages were inundated, and the water level was still growing. The urban flooding caused by this exceptional rainstorm has far exceeded the design capacity of the local flood control and drainage system. Floods exceeding the guaranteed level occurred in the Qihe River and the Communist Canal, and floods exceeding the alert level occurred in the Weihe River. The overflow resulted in the formation of obviously flooded areas after heavy rainfall mainly around the Weihe River, Communist Canal, and Qihe River, which aligns with the spatial distribution of our extraction result.

B. Measurement of Ground Deformation

The StaMPS/SBAS time-series InSAR processing was performed on the SAR images to obtain an annual average surface deformation rate map for the period January 2020 to April 2023, which includes the flood date of July 20, 2021, as shown in Fig. 5. The colors of the points represent their vertical deformation rates. Red points indicate ground subsidence, while blue points indicate land uplift. The surface subsidence area is unevenly distributed spatially and can be mainly divided into four regions labeled D1, D2, D3, and D4 in Fig. 5(a). There are two main factors of the ground subsidence, i.e., groundwater overexploitation and coal mining.

D1 with the most severe subsidence is mainly located in the eastern part of Handan City, Hebei Province. There is a lack of surface water resources in the urban area of Handan, and large-scale groundwater exploitation over a long period has formed a large groundwater level funnel around the 1970s. According to the 2022 statistics, the shallow groundwater overdraft zone within the city accounts for about half of the city's area. The continuous decline of the groundwater level tends to disrupt

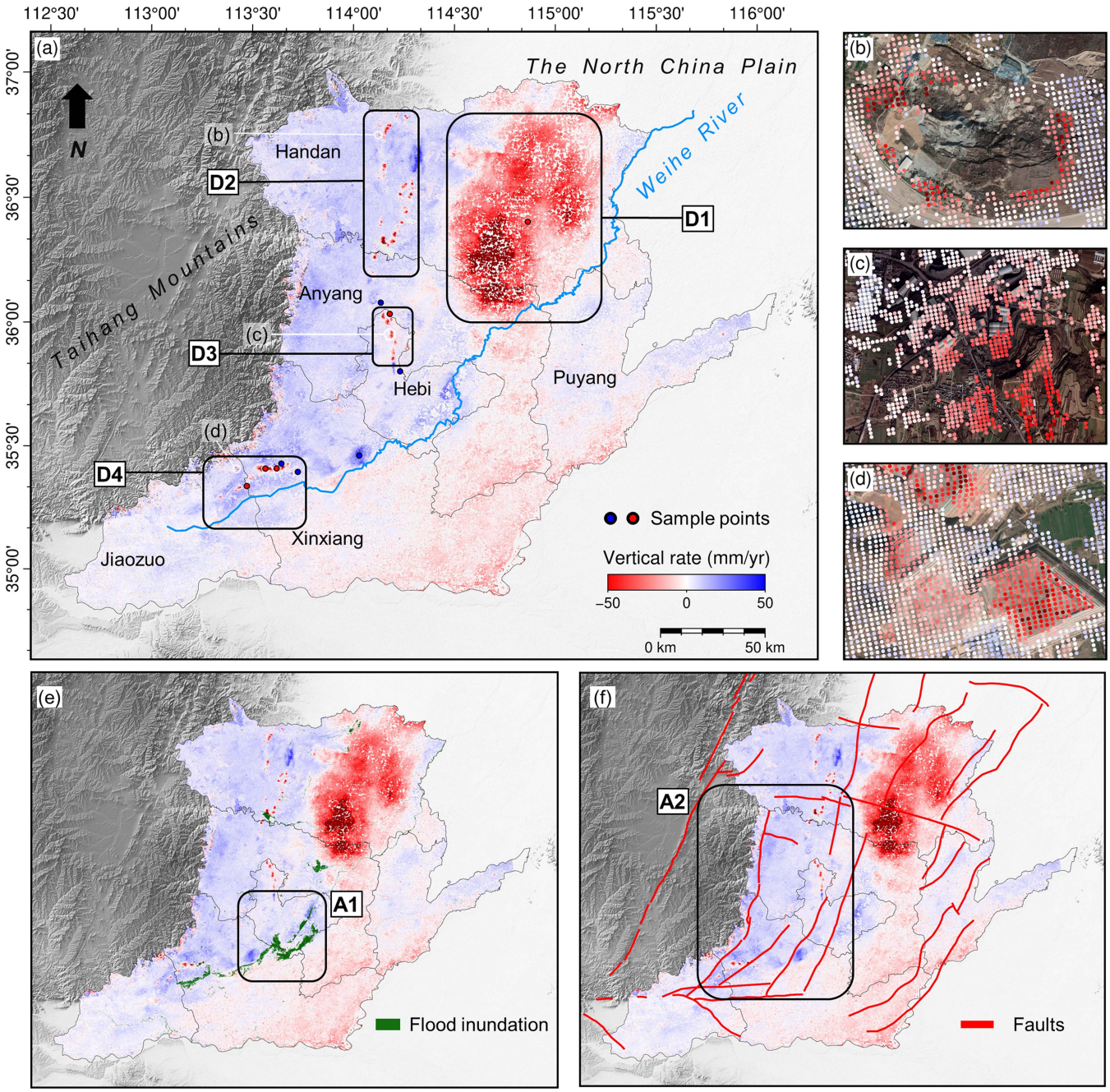

Fig. 5. InSAR-derived surface deformation rate map. (a) Distribution of the main subsidence areas D1, D2, D3, and D4, with some details in D2, D3, and D4 shown in (b), (c), and (d). As seen on the Google Maps optical image, (b) Presence of multiple traces of mining holes. (c) Multiple mining factories. (d) Open-pit mining sites. (e) and (f) show the distributions of major uplift areas A1 and A2.

the physical and chemical environment of the land, causing ground subsidence. The leading cause of ground subsidence can be considered to be the long-term exploitation of groundwater. Most of the subtle subsidence within Puyang and Anyang is also due to this reason.

D2 is located mainly in the western part of Handan City, Hebei Province; D3 is primarily in Hebi City, Henan Province; and D4 is mainly in Hui County, Xinxiang City. Their subsidence is sporadically distributed and close to the foothills of the Taihang Mountains, and the subsidence points are partly mining areas in addition to residential areas. The central subsidence area of D2 is located near Fengfeng Mining District, a major mining area in Handan City. Most subsidence points in D3 are located in Heshan District and Shancheng District in the north of Hebi, where extensive coal mining has been carried out since the last century. Various mineral resources are located in the premountainous of D4, and some subsidence points are located in mining areas. Mining is also a leading cause of ground subsidence. Coal mining destroys the stratigraphic structure and tends to cause surface subsidence; water is pumped out of the mines during

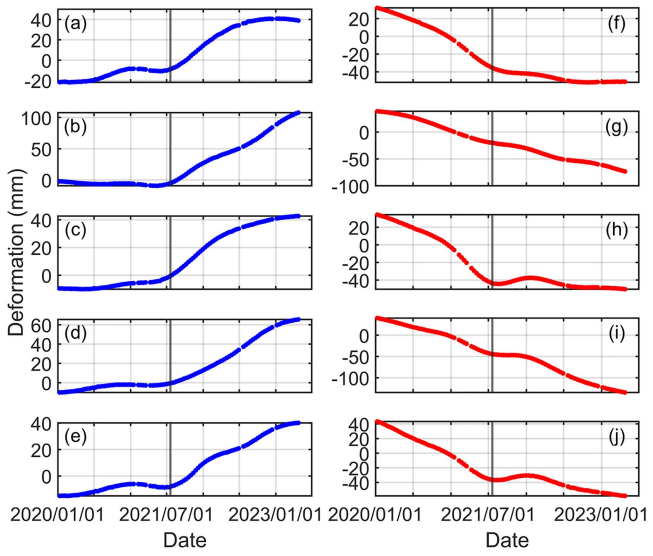

Fig. 6. (a)–(e) Deformation time series of five uplift sample points. (f)–(j) Deformation time series of five subsidence sample points. The black vertical lines in (a)–(j) represent the storm date of July 20, 2021. The locations of sample points were schematized with blue and red circles in Fig. 5, respectively.

the process, decreasing the local groundwater level. Therefore, subsidence in areas D2, D3, and D4 could be due to mining in addition to groundwater exploitation. The above-mentioned conclusions can also be corroborated with researches up to 2020 [21], [22].

It can be seen that the surface uplift area is mainly distributed in the vicinity of the Weihe River basin and the area in front of the Taihang Mountains. As shown in Fig. 5(e), the upstream section of Weihe River has obvious flooded areas, and the points located around the flooded areas in A1 show an uplift phenomenon. Fig. 5(f) shows there are several faults in the A2, and the points with uplift tendency have some spatial correlation with the distribution of the faults, but they are still mainly distributed in the section of the transition from the front of the Taihang Mountains to the plains.

Typical points in the subsidence and uplift regions were selected to observe the time series deformation trends, and the results obtained can be seen in Fig. 6. It is noteworthy that most of the points with uplift or subsidence trends have time series deformation curves with significant trend-changing phenomena near the date of the "7.20" Rainstorm Event. For about a year after the storm date, most of the points maintained the new deformation trend, and they showed a tendency to resume their original trend after one year. It can be assumed that the change in the trend is related to the rain, the effects of which diminish over time.

C. Detection of Storm-Affected Ground Deformation Areas

To identify areas where the trend of surface deformation has changed due to flooding, based on the time series pattern of typical points, it is possible to illustrate the spatial characteristics of the impact of the rainstorm and the flooding it brought by segmenting the time series of PS points at specific points in time and classifying them.

Considering 20 July as the date of the storm (t_{storm}), we classify the points into three classes.

1) Class I: Points with deformation rate (v_d) essentially smaller than zero before t_{storm} and about zero for a period after t_{storm} are considered to be areas where the effect of the flooding have resulted in the alleviation of ground subsidence.
2) Class II: Points with v_d equal to zero before t_{storm} and greater than zero for a period after t_{storm} are considered to be areas of ground uplift due to the effects of flooding.
3) Class III: The remaining points with deformation trend unaffected by flooding or where the main influence factor is not flooding.

The results are shown in Fig. 7; Class III is not labeled. We detect the points where the storm effect lasts up to six months after t_{storm} as in Fig. 7(a) and the points where the storm effect lasts up to one year after t_{storm} as Fig. 7(b), respectively. It can be tentatively observed that most of the point uplifts were short-term, and the number of points where the uplift lasted for a year has been considerably less than the number of points that lasted for half a year.

It can be concluded that the heavy precipitation affected the deformation trend of many subsiding points and even resulted in land uplift. Compared with the deformation rate map obtained in Section IV-B, a large number of nonsubsidence points produced an uplift trend that was not initially present, and the distribution of the uplift trend points in Fig. 5 is almost the same as the results shown in Fig. 7, which indicates that the uplifting trend points are the results of heavy precipitation. These points are more often located around the mountain front area.

For subsidence points, most were mitigated to varying degrees. However, there are many points in the subsidence area, especially in the severe subsidence area, such as the dark purple points in D1 in Fig. 7(a), that are not visibly affected, or where the effect is maintained for a short period of time and the original rate of subsidence is quickly resumed, as shown in Fig. 6(g). We can consider three main reasons as follows.

1) The mine has destroyed the local soil and water conservation capacity, and the short-term heavy precipitation had caused less recharge to the aquifer.
2) The long period of subsidence area's soil has been compacted before the rainstorm, which has formed permanent subsidence that can hardly be recovered.
3) Soils take longer to respond to groundwater recharge. Since the storm has been more than two years to date, we focus on its short-term apparent response to the storm.

D. Relationship Between Groundwater Change and Ground Deformation

Rainfall is the form of precipitation that recharges groundwater the most. Once the rainwater reaches the ground, one portion becomes surface runoff and the other contains groundwater infiltration recharge. Since surface water infiltration needs to go through the process of soil water saturation before it can

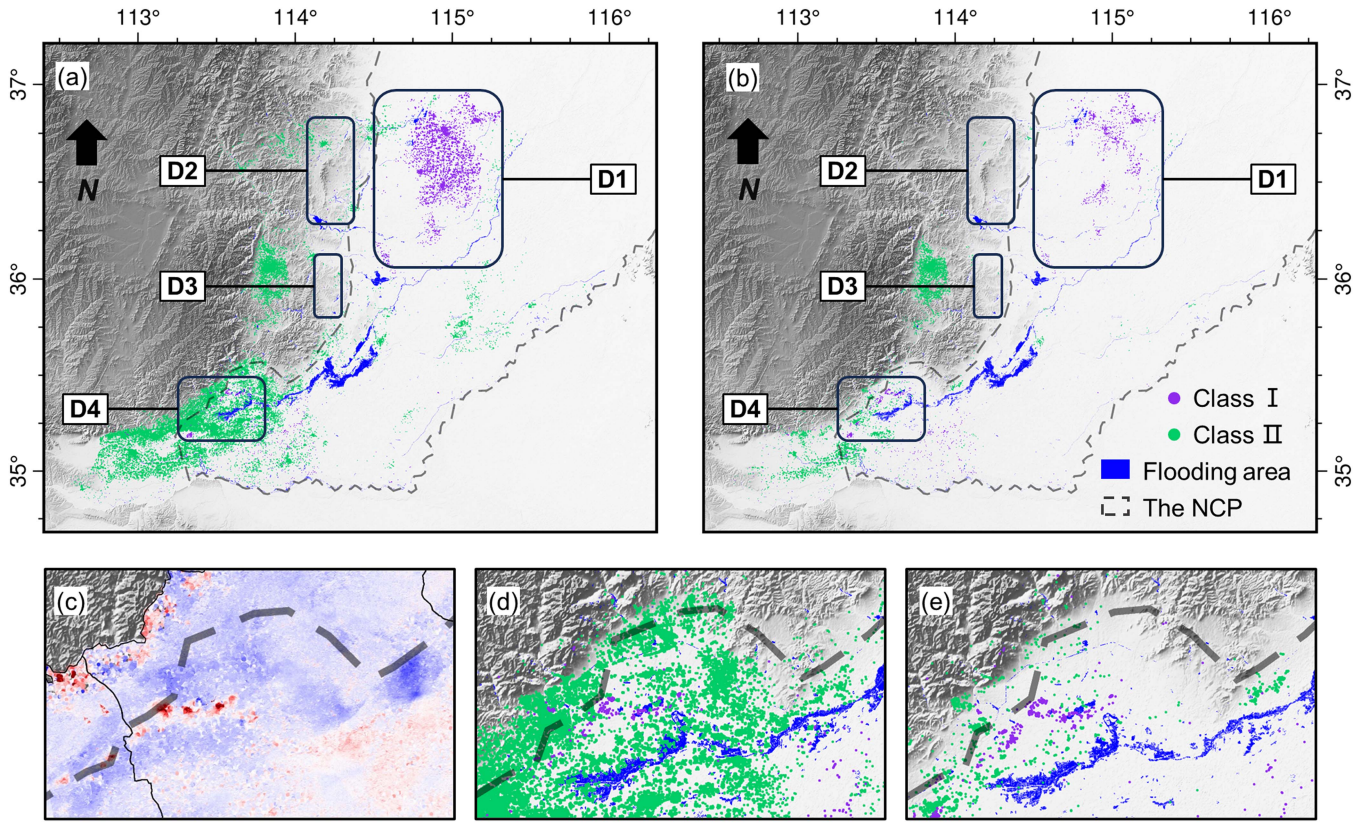

Fig. 7. Distribution of points of surface uplift due to the impact of heavy rainfall and flooding. (a) Points where the affected uplift effect lasted for half a year. (b) Points where the affected uplift effect lasted for one year. (c), (d), and (e) are the corresponding zoomed-in maps of D4. (c) Deformation rate extraction result. (d) Extraction result of the affected points within six months of the storm. (e) Extraction result of the affected points within one year of the storm.

be converted into groundwater, there is a response time for the groundwater level [40].

We selected relevant groundwater wells and observed the relationship between the time series trends of groundwater level, precipitation, and deformation time series, as shown in Fig. 8. Groundwater level data were measured every five days. Within less than five days, groundwater levels responded to heavy precipitation with a sharp rise, and the increasing trend stayed in place for anywhere from two to four months, lasting until November 2021. To Henan Province's official water monthly report data as a verification, if January 2020 as a reference level for comparison, the whole plain area of Henan Province in early August 2021 average groundwater level relative to the previous month's rose by 1.83 m, and the groundwater level in Hebi City alone rises to 5.45 m. The average water level for the entire Henan Province stopped increasing continuously in early November 2021, some cities' water levels continued rising until early December. The average water level in Henan Province after t_{storm} was higher than it before t_{storm} and has not yet dropped back to the lowest prestorm level until April 2023, although they both show a seasonal decrease trend. It suggests that there was significant groundwater recharge from the "7.20" Rainstorm Event.

The deformation trend of the subsidence points also changed drastically before and after the rainstorm date. The degree of subsidence decelerations varied after the rainstorm, with most of the points in the outer rim of the D1 subsidence funnel and D4 remaining decelerated for more than one year, and no apparent points in D2 and D3 being mitigated due to the poor soil and water capacity of the land, which is mainly caused by mining.

There is also significant subsidence deceleration or land uplift around some points in the center of D1 and the transition zone from the Taihang Mountains to the plains, with no flooding. These locations do not have rainwater accumulation but still can recharge groundwater through precipitation, in particular, the aquifer in front of the mountain has good permeability and surface rainwater can quickly infiltrate to replenish the aquifer. In addition, groundwater is interconnected, and groundwater recharged from neighboring areas can circulate. These allow points around nonflooded areas to cause surface uplift through groundwater recovery.

Regardless of the duration of mitigation, the trend-turning node is the date of the rainstorm. Overall, precipitation, groundwater levels, and surface deformation trends positively correlate. Groundwater recharge brought by heavy rainfall causes surface uplift, alleviating extensive ground subsidence.

V. Discussion

We focus on the effects of the heavy rainfall on ground subsidence in the "7.20" Rainstorm Event and find that the groundwater recovery by the rainstorm and floods it brought had

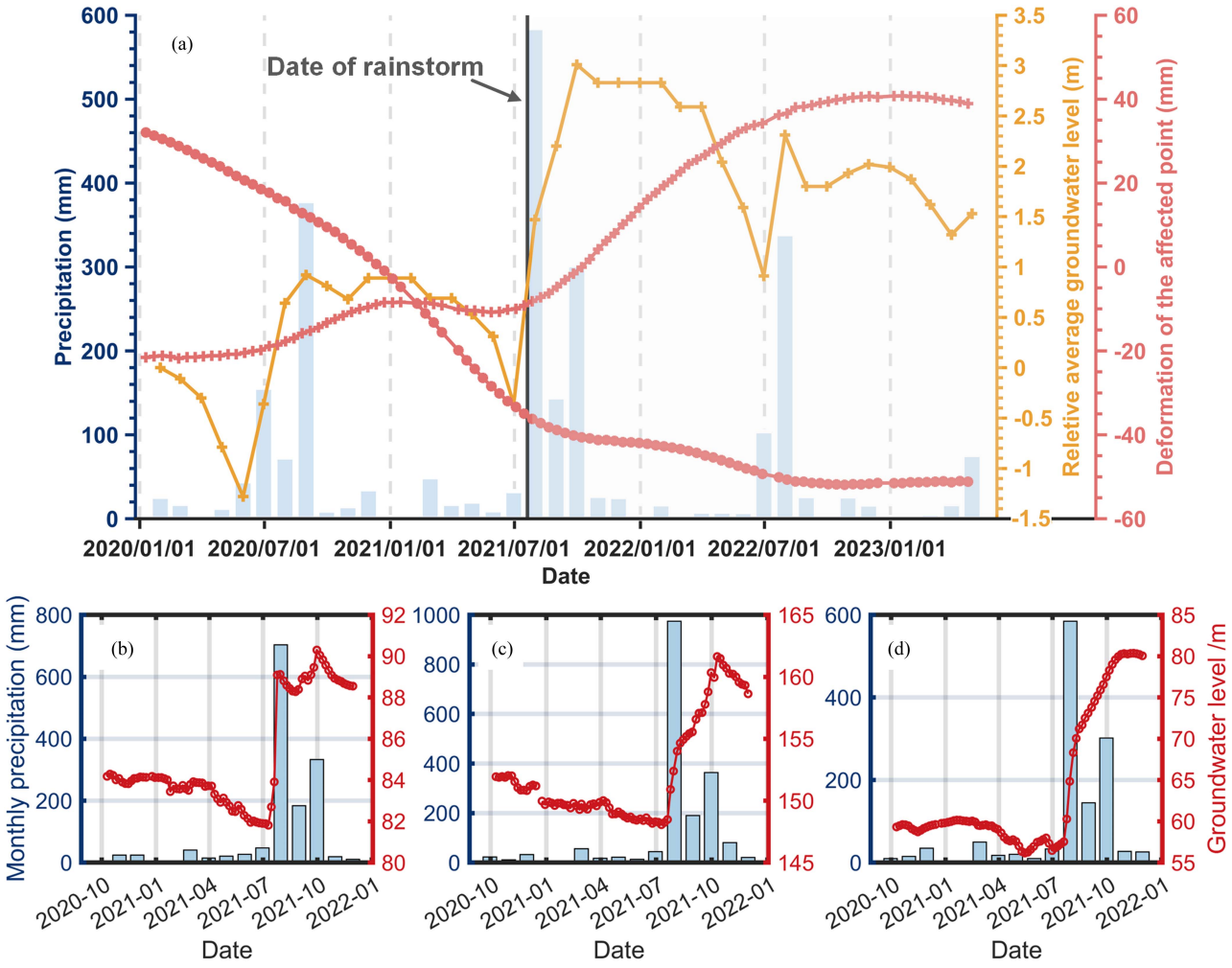

Fig. 8. Comparison of temporal trends in precipitation, groundwater level, and deformation time series. (a) Average groundwater level in the plains of the entire Henan Province superimposed on Fig. 6(a) and (f). (b), (c), and (d) Average monthly precipitation and five-day groundwater measurements at the sites in Jiaozuo, Hebi, and Xinxiang from September 2020 to November 2021, respectively.

affected surface deformation, leading to subsidence deceleration or even land uplift.

There are some limitations due to the inherent characteristics of the S1 data. In the process of flood inundation area extraction using SAR intensity images, the identified flood inundation extent may not be the maximum extent due to the long-time interval (12 days) of S1 data. The current booming SAR small-satellite constellation, which is capable of acquiring postdisaster images in a timely and high-frequency manner, can extract the process of flood growth and recession, which is even more helpful for disaster prevention and mitigation, postdisaster reconstruction and analysis of the ground subsidence and groundwater response.

The data acquisition time used in the InSAR deformation extraction spans before and after the flood inundation. Since water surfaces are noncoherent targets, flooding can cause inundated InSAR measurements to lose coherence over the inundation time period, and increased soil moisture may trigger more severe nonzero closure phases, potentially leading to biases in deformation estimates [41], [42].

The local soil conditions are an essential factor in storm flooding, affecting surface deformation. Differences in soil conditions can affect the process in the following ways. i) Storm flooding infiltration needs a process of surface soil water saturation, and the infiltration rate relates to soil porosity and other factors [43]. Thus, the rate of groundwater recovery from storm flooding varies. ii) After the groundwater level rises, the deformation of the sand layer is basically without hysteresis while the clayey soil layer's deformation hysteresis is evident [44]. The water-bearing sands become increasingly fine-grained from the mountain front to the plains [21]; therefore, the mountain front area has a shorter response to groundwater recharge due to heavy rainfall as well as surface uplift, which is shown as the number of points of the uplifted area is more distributed in the mountain front.

However, as with ground subsidence, unanticipated ground uplift can have as significant an impact on surface cities and economies as ground subsidence, resulting in many secondary disasters. The effect of storm flooding on ground deformation is a factor to be considered. Meanwhile, the trend of droughts

and floods in China has changed in recent years; there has been a flooding shift trend from south to north, with more frequent rainstorms in north China. From July 29 to August 1, 2023, under the influence of Super Typhoon Doksuri, Beijing–Tianjin–Hebei region in China experienced exceptionally heavy rainfall, with the amount of precipitation in Beijing reaching the largest in the 140-year history of instrumental measurement records. Water scarcity and groundwater overexploitation in the northern part of the NCP are more severe than in its southern region, where several large-scale ground subsidence funnels exist. Similar to the "7.20" Rainstorm Event, the flood brought by the rainstorm in 2023 may have a similar impact on the groundwater recovery and subsidence mitigation in cities, such as Beijing and the potential impact of surface uplift on urban transportation and building safety needs to be taken into account in the postdisaster remediation work.

VI. Conclusion

This study used SAR data's intensity and phase information to identify flood inundation and measure time series deformation, respectively. Taking the "7.20" Rainstorm Event in Henan Province, China, as an example, we employed the Sentinel-1 data to obtain the flood inundation area and three years' deformation around the rainstorm's date, and then analyzed the mechanism between groundwater recharge and subsidence mitigation under the influence of the storm event in conjunction with groundwater level changes. The main conclusions are as follows.

1) The water surface increased considerably at approximately 546.2 km^2 after the rain, and the flooded area was mainly distributed in the central part of the basins of the Communist Canal, Weihe River, and Qihe River, as well as in the northern part of the Yuecheng Reservoir area increased significantly.
2) The subsidence funnels, mainly caused by long-term groundwater overexploitation and subsurface resource mining, are distributed in the Shancheng District and Heshan District of Hebi City, Hui County of Xinxiang City, and the northern part of Anyang City connecting to Handan City. From January 2020 to April 2023, the maximum vertical subsidence rate was about 167.7 mm/yr.
3) The "7.20" Rainstorm Event recharged the aquifer, and the groundwater level less than five days after the rainstorm time began to rise sharply. The Groundwater recovery leads to a widespread phenomenon of subsidence deceleration or even land uplift around the flooded areas and in mountain front areas.

This study provides a valuable technical reference for similar scenes, such as the 2023 heavy rain event in China's Beijing–Tianjin–Hebei region with severe land subsidence.

Acknowledgment

The authors would like to thank Andrew Hooper for sharing the StaMPS program, the European Space Agency (ESA) for providing the Sentinel-1 data under the framework of the Sino-EU Dragon Project (id 59332), the Japan Aerospace Exploration Agency (JAXA) for providing the AW3D DEM, the China Geological Survey (CGS), the Water Resources Department of Henan Province for providing the groundwater level data, and the China Meteorological Data Service Center for providing the precipitation data.

References

[1] S. N. Jonkman, "Global perspectives on loss of human life caused by floods," *Natural Hazards*, vol. 34, no. 2, pp. 151–175, Feb. 2005, doi: 10.1007/s11069-004-8891-3.
[2] Ministry of Emergency Management of the Peoples Republic of China, "Emergency management releases nation's top 10 natural disasters for 2021," Accessed: Jan. 9, 2024. [Online]. Available: https://www.mem.gov.cn/xw/yjglbgzdt/202201/t20220123_407199.shtml
[3] Q. Zhang, R. Li, J. Sun, F. Lu, J. Xu, and F. Zhang, "A review of research on the record-breaking precipitation event in Henan province, China, July 2021," *Adv. Atmos. Sci.*, vol. 40, no. 8, pp. 1485–1500, Aug. 2023, doi: 10.1007/s00376-023-2360-y.
[4] Z. Li et al., "Rapid assessment of traffic inefficiency under flood scenarios over wide regions," *Geomatics Inf. Sci. Wuhan Univ.*, vol. 48, no. 7, pp. 1039–1049, 2023, doi: 10.13203/j.whugis20220512.
[5] J. Li et al., "Satellite detection of surface water extent: A review of methodology," *Water*, vol. 14, no. 7, Apr. 2022, Art. no. 1148, doi: 10.3390/w14071148.
[6] S. Martinis et al., "Comparing four operational SAR-based water and flood detection approaches," *Int. J. Remote Sens.*, vol. 36, no. 13, pp. 3519–3543, Jul. 2015, doi: 10.1080/01431161.2015.1060647.
[7] S. Dellepiane, G. Bo, S. Monni, and C. Buck, "SAR images and interferometric coherence for flood monitoring," in *Proc. IEEE Int. Geosci. Remote Sens. Symp. Taking Pulse Planet: Role Remote Sens. Manag. Environ.*, 2000, pp. 2608–2610, doi: 10.1109/IGARSS.2000.859656.
[8] G. Nico, M. Pappalepore, G. Pasquariello, A. Refice, and S. Samarelli, "Comparison of SAR amplitude vs. coherence flood detection methods - a GIS application," *Int. J. Remote Sens.*, vol. 21, no. 8, pp. 1619–1631, Jan. 2000, doi: 10.1080/014311600209931.
[9] J. Wang et al., "Flood inundation region extraction method based on Sentinel-1 SAR data," *J. Catastrophology*, vol. 36, no. 4, pp. 214–220, 2021.
[10] Y. Xue, Y. Zhang, S. Ye, J. Wu, and Q. Li, "Land subsidence in China," *Environ. Geol.*, vol. 48, no. 6, pp. 713–720, Sep. 2005, doi: 10.1007/s00254-005-0010-6.
[11] J. Pacheco-Martínez et al., "Land subsidence and ground failure associated to groundwater exploitation in the Aguascalientes Valley, México," *Eng. Geol.*, vol. 164, pp. 172–186, Sep. 2013, doi: 10.1016/j.enggeo.2013.06.015.
[12] R. L. Hu, Z. Q. Yue, L. C. Wang, and S. J. Wang, "Review on current status and challenging issues of land subsidence in China," *Eng. Geol.*, vol. 76, no. 1/2, pp. 65–77, Dec. 2004, doi: 10.1016/j.enggeo.2004.06.006.
[13] A. Hooper, D. Bekaert, K. Spaans, and M. Arıkan, "Recent advances in SAR interferometry time series analysis for measuring crustal deformation," *Tectonophysics*, vol. 514–517, pp. 1–13, Jan. 2012, doi: 10.1016/j.tecto.2011.10.013.
[14] T. J. Wright, "Toward mapping surface deformation in three dimensions using InSAR," *Geophysical Res. Lett.*, vol. 31, no. 1, 2004, Art. no. L01607, doi: 10.1029/2003GL018827.
[15] B. Wang, C. Zhao, Q. Zhang, Z. Lu, and A. Pepe, "Long-term continuously updated deformation time series from multisensor InSAR in Xi'an, China from 2007 to 2021," *IEEE J. Sel. Topics Appl. Earth Observ. Remote Sens.*, vol. 14, pp. 7297–7309, 2021, doi: 10.1109/JSTARS.2021.3096996.
[16] Y. Wang et al., "Using TerraSAR X-band and Sentinel-1 C-band SAR interferometry for deformation along Beijing-Tianjin intercity railway analysis," *IEEE J. Sel. Topics Appl. Earth Observ. Remote Sens.*, vol. 14, pp. 4832–4841, 2021, doi: 10.1109/JSTARS.2021.3076244.
[17] L. Zhu et al., "Land subsidence due to groundwater withdrawal in the Northern Beijing plain, China," *Eng. Geol.*, vol. 193, pp. 243–255, Jul. 2015, doi: 10.1016/j.enggeo.2015.04.020.
[18] A. Ferretti, C. Prati, and F. Rocca, "Permanent scatterers in SAR interferometry," *IEEE Trans. Geosci. Remote Sens.*, vol. 39, no. 1, pp. 8–20, Jan. 2001, doi: 10.1109/36.898661.
[19] P. Berardino, G. Fornaro, R. Lanari, and E. Sansosti, "A new algorithm for surface deformation monitoring based on small baseline differential SAR interferograms," *IEEE Trans. Geosci. Remote Sens.*, vol. 40, no. 11, pp. 2375–2383, Nov. 2002, doi: 10.1109/TGRS.2002.803792.

[20] M. Shi, H. Gong, M. Gao, B. Chen, S. Zhang, and C. Zhou, "Recent ground subsidence in the North China Plain, China, revealed by Sentinel-1A datasets," *Remote Sens.*, vol. 12, no. 21, Oct. 2020, Art. no. 3579, doi: 10.3390/rs12213579.
[21] Y. Li, X. Zuo, P. Xiong, Z. Chen, F. Yang, and X. Li, "Monitoring land subsidence in North-central Henan Plain using the SBAS-InSAR method with Sentinel-1 imagery data," *J. Indian Soc. Remote Sens.*, vol. 50, no. 4, pp. 635–655, Apr. 2022, doi: 10.1007/s12524-021-01484-6.
[22] L. Dong, C. Wang, Y. Tang, H. Zhang, W. Duan, and W. Jing, "Sentinel-1 InSAR measurements of land subsidence over Henan province, China from 2018 to 2020," in *Proc. SAR Big Data Era*, 2021, pp. 1–4, doi: 10.1109/BIGSARDATA53212.2021.9574177.
[23] G. Zhang, Y. Fei, Y. Tian, Q. Wang, and M. Yan, "Characteristics of alleviating the over-exploitation and its recharge on the rainstorm flood to the shallow groundwater in the southern plain of Haihe River basin," *J. Hydraulic Eng.*, vol. 46, no. 5, pp. 594–601, 2015, doi: 10.13243/j.cnki.slxb.20140990.
[24] S. Ye, Y. Xue, J. Wu, X. Yan, and J. Yu, "Progression and mitigation of land subsidence in China," *Hydrogeology J.*, vol. 24, no. 3, pp. 685–693, May 2016, doi: 10.1007/s10040-015-1356-9.
[25] Ministry of Natural Resources of the People's Republic of China, "Circular of the ministry of land and resources and the ministry of water resources on the issuance of the national plan for prevention and control of ground subsidence (2011-2020)," Accessed: Jan. 9, 2024. [Online]. Available: http://f.mnr.gov.cn/202103/t20210308_2616738.html
[26] J. W. Bell, F. Amelung, A. Ferretti, M. Bianchi, and F. Novali, "Permanent scatterer InSAR reveals seasonal and long-term aquifer-system response to groundwater pumping and artificial recharge: Permanent scatterer InSAR," *Water Resour. Res.*, vol. 44, no. 2, Feb. 2008, doi: 10.1029/2007WR006152.
[27] Y.-Y. Lu, C.-Q. Ke, H.-J. Jiang, and D.-L. Chen, "Monitoring urban land surface deformation (2004–2010) from InSAR, groundwater and levelling data: A case study of Changzhou city, China," *J. Earth Syst. Sci.*, vol. 128, no. 6, pp. 1–15, Aug. 2019, doi: 10.1007/s12040-019-1173-y.
[28] M. Darvishi, G. Destouni, S. Aminjafari, and F. Jaramillo, "Multi-sensor InSAR assessment of ground deformations around lake mead and its relation to water level changes," *Remote Sens.*, vol. 13, no. 3, pp. 1–18, Jan. 2021, doi: 10.3390/rs13030406.
[29] S. L. Mouélic, D. Raucoules, C. Carnec, C. King, and F. Adragna, "A ground uplift in the city of Paris (France) detected by satellite radar interferometry: Ground uplift in Paris detected by InSAR," *Geophysical Res. Lett.*, vol. 29, no. 17, pp. 34–31, Sep. 2002, doi: 10.1029/2002GL015630.
[30] S. Coda, S. Tessitore, D. Di Martire, D. Calcaterra, P. De Vita, and V. Allocca, "Coupled ground uplift and groundwater rebound in the metropolitan city of Naples (Southern Italy)," *J. Hydrol.*, vol. 569, pp. 470–482, Feb. 2019, doi: 10.1016/j.jhydrol.2018.11.074.
[31] J. Liang and D. Liu, "A local thresholding approach to flood water delineation using Sentinel-1 SAR imagery," *Int. Soc. Photogrammetry Remote Sens. J. Photogrammetry Remote Sens.*, vol. 159, pp. 53–62, Jan. 2020, doi: 10.1016/j.isprsjprs.2019.10.017.
[32] S. Jia, D. Xue, C. Li, J. Zheng, and W. Li, "Study on new method for water area information extraction based on Sentinel-1 data," *Yangtze River*, vol. 50, no. 2, pp. 213–217, 2019, doi: 10.16232/j.cnki.1001-4179.2019.02.038.
[33] S. Martinis, A. Twele, and S. Voigt, "Towards operational near real-time flood detection using a split-based automatic thresholding procedure on high resolution TerraSAR-X data," *Natural Hazards Earth Syst. Sci.*, vol. 9, no. 2, pp. 303–314, Mar. 2009, doi: 10.5194/nhess-9-303-2009.
[34] S. Chen, W. Huang, Y. Chen, and M. Feng, "An adaptive thresholding approach toward rapid flood coverage extraction from Sentinel-1 SAR imagery," *Remote Sens.*, vol. 13, no. 23, Dec. 2021, Art. no. 4899, doi: 10.3390/rs13234899.
[35] J.-S. Lee, "Refined filtering of image noise using local statistics," *Comput. Graph. Image Process.*, vol. 15, no. 4, pp. 380–389, Apr. 1981.
[36] C. Werner, U. Wegmüller, T. Strozzi, and A. Wiesmann, "GAMMA SAR and interferometric processing software," in *Proc. Ers-Envisat Symp.*, 2000, vol. 1620, Art. no. 1620.
[37] A. Hooper, P. Segall, and H. Zebker, "Persistent scatterer interferometric synthetic aperture radar for crustal deformation analysis, with application to Volcán Alcedo, Galápagos," *J. Geophys. Res.*, vol. 112, no. B7, Jul. 2007, Art. no. B07407, doi: 10.1029/2006JB004763.
[38] A. Hooper, "A multi-temporal InSAR method incorporating both persistent scatterer and small baseline approaches," *Geophys. Res. Lett.*, vol. 35, no. 16, Aug. 2008, Art. no. L16302, doi: 10.1029/2008GL034654.
[39] N. Xu, "Reflections on the '721' rainstorm flooding of Weihe River," *Haihe Water Resour.*, no. 1, pp. 42–45, 2022.
[40] C.-D. Jan, T.-H. Chen, and W.-C. Lo, "Effect of rainfall intensity and distribution on groundwater level fluctuations," *J. Hydrol.*, vol. 332, no. 3/4, pp. 348–360, Jan. 2007, doi: 10.1016/j.jhydrol.2006.07.010.
[41] F. De Zan, A. Parizzi, P. Prats-Iraola, and P. Lopez-Dekker, "A SAR interferometric model for soil moisture," *IEEE Trans. Geosci. Remote Sens.*, vol. 52, no. 1, pp. 418–425, Jan. 2014, doi: 10.1109/TGRS.2013.2241069.
[42] F. De Zan, M. Zonno, and P. Lopez-Dekker, "Phase inconsistencies and multiple scattering in SAR interferometry," *IEEE Trans. Geosci. Remote Sens.*, vol. 53, no. 12, pp. 6608–6616, Dec. 2015, doi: 10.1109/TGRS.2015.2444431.
[43] M. N. Viswanathan, "Recharge characteristics of an unconfined aquifer from the rainfall-water table relationship," *J. Hydrol.*, vol. 70, no. 1–4, pp. 233–250, Feb. 1984, doi: 10.1016/0022-1694(84)90124-0.
[44] H. Guo et al., "The evolution characteristics and mechanism of the land subsidence in typical areas of the North China Plain," *Geol. China*, vol. 44, no. 6, pp. 1115–1127, 2017.

Qianye Lan received the B.Eng. degree in remote sensing science and technology from Wuhan University, Wuhan, China, in 2023. She is currently working toward the M.Eng. degree in remote sensing science and technology with the State Key Laboratory of Information Engineering in Surveying, Mapping and Remote Sensing, Wuhan University.

Her research interests include atmospheric correction, deformation measurement, and related applications in the InSAR field.

Jie Dong received the B.Eng. degree in surveying and mapping engineering from the China University of Mining and Technology, Xuzhou, China, in 2011, the M.A. degree in geodesy and survey engineering from Hohai University, Nanjing, China, in 2014, and the Ph.D. degree in photogrammetry and remote sensing from the State Key Laboratory of Information Engineering in Surveying, Mapping and Remote Sensing, Wuhan University, Wuhan, China, in 2018.

Since 2018, he has been with the School of Remote Sensing and Information Engineering, Wuhan University. His research interests include multitemporal interferometric synthetic aperture radar algorithms and geological disaster monitoring.

Shangjing Lai received the B.S. degree in geomatics engineering from Southeast University, Nanjing, China, in 2019, and the M.Eng. degree in geomatics engineering from the State Key Laboratory of Information Engineering in Surveying, Mapping, and Remote Sensing, Wuhan University, Wuhan, China, in 2021, where she is currently working toward the Ph.D. degree in photogrammetry and remote sensing.

Her research focuses on hydrogeological studies based on time-series InSAR analysis.

Nan Wang received the B.S. degree in geographical information system from the Taiyuan University of Technology, Taiyuan, China, in 2016; the M.Eng. degree in surveying and mapping engineering and the Ph.D. degree in photogrammetry and remote sensing from the State Key Laboratory of Information Engineering in Surveying, Mapping and Remote Sensing, Wuhan University, Wuhan, China, in 2018 and 2023, respectively.

Her research focuses on time-series InSAR analysis and infrastructure monitoring.

Lu Zhang received the B.Eng. and M.Eng. degrees in computer science and technology from the Wuhan University of Hydraulic and Electrical Engineering, Wuhan, China, in 1997 and 2000, respectively, and the Ph.D. degree in photogrammetry and remote sensing from Wuhan University, Wuhan, in 2005.

From 2005 to 2007, he was a Postdoctoral Research Fellow with the Institute of Space and Earth Information Science, Chinese University of Hong Kong, Hong Kong. Since 2007, he has been with the State Key Laboratory of Surveying, Mapping, and Remote Sensing, Wuhan University, where he became a Full Professor in 2013. He was involved in several research projects funded by the National Natural Science Foundation of China and Ministry of Science and Technology. In recent years, he has authored or coauthored more than 40 peer-reviewed scientific papers. His research interests include synthetic aperture radar interferometry as well as remote sensing classification and change detection.

Mingsheng Liao received the B.S. degree in electronic engineering from the Wuhan Technical University of Surveying and Mapping (WTUSM), Wuhan, China, in 1982, the M.A. degree in electronic and information engineering from the Huazhong University of Science and Technology, Wuhan, China, in 1985, and the Ph.D. degree in photogrammetry and remote sensing from WTUSM, in 2000.

He is the Principal Investigator of several projects funded by the Ministry of Science and Technology (MOST), China, and the National Natural Science Foundation of China. Since 1997, he has been a Professor with the State Key Laboratory of Information Engineering in Surveying, Mapping and Remote Sensing, Wuhan University, Wuhan. Since 2004, he has been the Principal Investigator of the ESA-MOST Cooperative Dragon project. His research interests include algorithms for interferometric synthetic aperture radar, integration and fusion of multisource spatial information, and applications of remote sensing data.